GEOPHYSICS, VOL. 69, NO. 4 (JULY-AUGUST 2004); P. 1017–1024, 19 FIGS.
10.1190/1.1778244

Amplitude and kinematic corrections of migrated images for nonunitary imaging operators

Antoine Guitton*

ABSTRACT

Obtaining migrated images with meaningful amplitudes is a challenging problem when the migration operator is not unitary. One possible solution to this problem is iterative inversion. However, inversion is an expensive process that can be rather difficult to apply, especially with 3D data. In this paper, I propose estimating migrated images similar to the least-squares inverse images by approximating the inverse Hessian, thus avoiding the need for iterative inversion. The inverse Hessian is approximated with a bank of nonstationary matching filters. These filters are not exact impulse responses and are limited in their ability to mimic the full effects of least-squares inversion. Tests on two data sets show that this filtering approach gives results similar to iterative least-squares inversion at a lower cost. This technique is flexible enough to be applied to images migrated from zero-offset or angle-domain common-image-point gathers.

INTRODUCTION

It is well known that most of the operators used for seismic processing are nonunitary (Claerbout, 1992). This means that for any operator $\mathbf{L}$, $\mathbf{L}'\mathbf{L} \neq \mathbf{I}$, where $(')$ stands for the adjoint and $\mathbf{I}$ is the identity matrix. A well-known nonunitary operator is the slant-stack operator where artifacts are created in both data space and model space when a limited range of offsets and ray parameters are used for the transformation (Kostov, 1990). For migration, because of the limited aperture of the acquisition geometry, the final migrated image can be blurred with uneven amplitudes (Gray, 1997).

Different approaches have been proposed to correct for amplitude effects during the migration process. Bleistein (1987), based on earlier work by Beylkin (1985), derived an inverse operator for Kirchhoff migration assuming infinite receiver coverage at the surface. A similar path is followed by Thierry et al. (1999) with the addition of nonlinear inversion with an approximated Hessian. Least-squares migration with regularization has proved effective with incomplete surface data (e.g., Nemeth et al., 1999) and irregular subsurface illumination due to complex structures (e.g., Prucha et al., 1999; Kuhl and Sacchi, 2001). Hu et al. (2001) introduced a deconvolution operator that approximates the inverse of the Hessian in the least-squares estimate of the migrated image. However, this method assumes a $v(z)$ medium, which means that the deconvolution operators are horizontally invariant. Rickett (2003) proposed estimating weighting functions from reference images to compensate illumination effects for finite-frequency depth migration.

In this paper, I propose a new strategy for approximating the inverse of the Hessian. This approach aims to estimate a bank of nonstationary matching filters (Rickett et al., 2001) between two migrated images that theoretically embed the effects of the Hessian. This approach is carried out after migration and is very cheap to apply. It can be applied to images migrated at zero-offset or to angle-domain common-image gathers. I illustrate this method with two data sets where the earth's reflectivity is estimated. The first data set is a flat-layer model with a complex velocity field; the second is the Marmousi data set (Bourgeois et al., 1991). I demonstrate that this approach can effectively recover amplitudes almost identical to the ones obtained with least-squares inversion at a much reduced cost.

THEORY

In this section, I show how the least-squares estimate of a migrated image can be approximated using nonstationary matching filters. Given a vector of seismic data $\mathbf{d}$ and a linear modeling operator $\mathbf{L}$, we seek a model of the earth $\mathbf{m}$ such that the length of a residual vector $\mathbf{r_d}(\mathbf{m})$ is minimized:

$$\mathbf{0} \approx \mathbf{r_d}(\mathbf{m}) = \mathbf{Lm} - \mathbf{d}. \tag{1}$$

Equation (1) is called a fitting goal. It states the need for the model $\mathbf{m}$ to best represent the data $\mathbf{d}$ using the modeling operator $\mathbf{L}$, independent of any norm. The model of the earth

Presented at the 73rd Annual Meeting, SEG. Published on Geophysics Online March 31, 2004. Manuscript received by the Editor November 6, 2003; revised manuscript received March 2, 2004.
*Stanford University, Stanford Exploration Project, Department of Geophysics, Mitchell Building, Stanford, California 94305-2215. E-mail: antoine@sep.stanford.edu.

$\mathbf{m}$ can be parameterized in terms of reflectivity or impedance as a function of depth or time. In this paper, I estimate the earth's reflectivity as a function of depth. The vector $\mathbf{d}$ can be poststack or prestack data, in two dimensions or in three. I will illustrate the proposed method with poststack and prestack 2D data. The linear modeling operator $\mathbf{L}$ is mathematically related to the migration operator by the adjoint state (Claerbout, 1985). Therefore, the migration operator is the adjoint of the modeling operator $\mathbf{L}$ such that (Claerbout, 1985)

$$\mathbf{L}'\mathbf{d} = \mathbf{m_1} \tag{2}$$

describes the migration process from the data vector $\mathbf{d}$ to an image $\mathbf{m_1}$. No assumptions are made about the migration operator $\mathbf{L}'$. This operator can be Kirchhoff migration (Nemeth et al., 1999) or a downward continuation method (Prucha et al., 1999). For migration, a model styling goal (regularization) is necessary to compensate for irregular geometry artifacts and uneven illumination (Prucha et al., 1999). Kuhl and Sacchi (2003) showed that ray-parameter smoothing reduces inversion artifacts significantly. I omit the regularization in my derivations and focus on the data-fitting goal in equation (1) only. By estimating $\mathbf{m}$ in a least-squares sense, we want to minimize the objective function:

$$f(\mathbf{m}) = \|\mathbf{r_d}\|^2 = \|\mathbf{Lm} - \mathbf{d}\|^2, \tag{3}$$

where $\|\cdots\|$ is the ℓ^2 norm. The least-squares estimate $\hat{\mathbf{m}}$ of the model is then given by

$$\hat{\mathbf{m}} = (\mathbf{L}'\mathbf{L})^{-1}\mathbf{L}'\mathbf{d}, \tag{4}$$

where $\mathbf{L}'\mathbf{L}$ is called the Hessian of $f(\mathbf{m})$. The inverse of the Hessian $(\mathbf{L}'\mathbf{L})^{-1}$ can be regarded as a deconvolution operator (Hu et al., 2001) that corrects the amplitudes of the final image. Unfortunately, with migration operators, the Hessian cannot generally be inverted, and iterative procedures such as conjugate gradient (CG) or the Newton method are often used (Lambaré et al., 1992). Yet, iterative methods are still very expensive to apply, and inversion is still far from being a commodity in the processing toolbox. The next section shows how we can approximate the effects of the Hessian with nonstationary matching filters, thus simulating the effects of least-squares inversion at a much reduced cost.

Approximating the Hessian

I replace $\mathbf{L}'\mathbf{d}$ with $\mathbf{m_1}$ in equation (4) to obtain

$$\hat{\mathbf{m}} = (\mathbf{L}'\mathbf{L})^{-1}\mathbf{m_1}. \tag{5}$$

In equation (5), $\hat{\mathbf{m}}$ and $\mathbf{L}'\mathbf{L}$ are unknown. Since I am looking for an approximation of the Hessian, I want to find two known images that are related by the same expression as in equation (5). This can be easily achieved by remodeling the data from $\mathbf{m_1}$ with $\mathbf{L}$, i.e.,

$$\mathbf{d_1} = \mathbf{Lm_1}, \tag{6}$$

and remigrating them with $\mathbf{L}'$ as follows:

$$\mathbf{m_2} = \mathbf{L}'\mathbf{d_1} = \mathbf{L}'\mathbf{Lm_1}. \tag{7}$$

It is easy to transform equation (7) into

$$\mathbf{m_1} = (\mathbf{L}'\mathbf{L})^{-1}\mathbf{m_2}, \tag{8}$$

which is very similar to equation (5). Note that $\mathbf{m_1}$ and $\mathbf{m_2}$ have a mathematical significance: they are both vectors of the Krylov subspace for the operator $\mathbf{L}$ and the data $\mathbf{d}$. Now I assume that we can write the inverse Hessian as a linear operator $\mathbf{B_0}$ such that equation (5) can be written as

$$\hat{\mathbf{m}} = \mathbf{B_0}\mathbf{m_1}, \tag{9}$$

and equation (8) as

$$\mathbf{m_1} = \mathbf{B_0}\mathbf{m_2}, \tag{10}$$

where $\mathbf{B_0} = (\mathbf{L}'\mathbf{L})^{-1}$. In equation (10), both $\mathbf{m_1}$ and $\mathbf{m_2}$ are known, but $\mathbf{B_0}$ is not. The idea of this paper is to approximate $\mathbf{B_0}$ with a bank of nonstationary filters $\mathbf{B}$ that will take us from $\mathbf{m_2}$ to $\mathbf{m_1}$ in equation (10) and from $\mathbf{m_1}$ to something similar to $\hat{\mathbf{m}}$ in equation (9). Therefore, I approximate the Hessian with a bank of matching filters $\mathbf{B}$ that are very easy and cheap to estimate. Choosing matching filters reflects the general idea that the Hessian is a transform operator between two similar images. My hope is not to perfectly represent the Hessian, but to improve the migrated image at a lower cost than least-squares migration.

Now I describe how the matching filters are estimated. Replacing $\mathbf{B_0}$ with $\mathbf{B}$ gives a new fitting goal where the length of a residual vector $\mathbf{r_{m_1}}(\mathbf{B})$ is minimized:

$$\mathbf{0} \approx \mathbf{r_{m_1}}(\mathbf{B}) = \mathbf{m_1} - \mathbf{Bm_2}. \tag{11}$$

Margrave (1998) and Rickett et al. (2001) show that equation (11) can be rewritten as follows:

$$\mathbf{0} \approx \mathbf{r_{m_1}}(\mathbf{b}) = \mathbf{m_1} - \mathbf{M_2}\mathbf{b}, \tag{12}$$

where $\mathbf{M_2}$ is the matrix form of the nonstationary convolution with $\mathbf{m_2}$, and $\mathbf{b}$ is the vector of unknown filter coefficients. Because we have many unknown filter coefficients in $\mathbf{b}$, I introduce in equation (11) a regularization term that penalizes differences between filter coefficients:

$$\begin{aligned} \mathbf{0} &\approx \mathbf{r_{m_1}} = \mathbf{m_1} - \mathbf{M_2}\mathbf{b}, \\ \mathbf{0} &\approx \mathbf{r_b} = \mathbf{Rb}, \end{aligned} \tag{13}$$

where $\mathbf{R}$ is the helix derivative (Claerbout, 1998). Note that the helix derivative corresponds to the spectral factorization of the 2D Laplacian operator $\nabla^2 = (\partial^2/\partial x^2 + \partial^2/\partial z^2)$ into a minimum phase filter, where x is the midpoint axis and z the depth axis (Fomel et al., 2003). Other familiar operators such as a 2D gradient $\nabla = (\partial/\partial x, \partial/\partial z)$ can be used instead. I estimate $\mathbf{b}$ in equation (13) in a least-squares sense by minimizing the objective function

$$f(\mathbf{b}) = \|\mathbf{r_{m_1}}\|^2 + \epsilon^2\|\mathbf{r_b}\|^2, \tag{14}$$

where ϵ is a trade-off parameter between data fitting and smoothing of the filter coefficients. The least-squares inverse is thus given by

$$\hat{\mathbf{b}} = \left(\mathbf{M_2'}\mathbf{M_2} + \epsilon^2\mathbf{R}'\mathbf{R}\right)^{-1}\mathbf{M_2'}\mathbf{m_1}. \tag{15}$$

The filter estimation process is similar to the one proposed by Rickett et al. (2001) for the adaptive subtraction of multiples. For this problem, I estimate 2D filters with helical boundary conditions (Mersereau and Dudgeon, 1974; Claerbout, 1998). One advantage of the helix is that it transforms the 2D filter estimation step into a 1D problem. The 2D filters can be also

estimated in patches with one stationary filter per patch. However, as opposed to stationary filters in patches, nonstationary filters can change continuously along the depth and midpoint axes, thus creating smooth results. Getting similar smoothness with stationary filters in patches would be more difficult because of the transition problems inside the window overlap zones (Guitton and Verschuur, 2004). Once the filters $\hat{\mathbf{b}}$ are estimated, the final image is obtained by computing

$$\hat{\mathbf{m}} \approx \mathbf{M_1}\hat{\mathbf{b}} = \hat{\mathbf{B}}\mathbf{m_1}, \tag{16}$$

where $\mathbf{M_1}$ and $\hat{\mathbf{B}}$ are the the convolutional operators with $\mathbf{m_1}$ and $\hat{\mathbf{b}}$, respectively.

Therefore, I propose the following algorithm for approximating the Hessian and obtaining better migrated images:

1) Compute a migrated image $\mathbf{m_1} = \mathbf{L}'\mathbf{d}$.
2) Compute a second image $\mathbf{m_2} = \mathbf{L}'\mathbf{L}\mathbf{m_1}$.
3) Estimate a bank of nonstationary matching filters $\hat{\mathbf{b}}$ [equation (15)].
4) Convolve $\hat{\mathbf{B}}$ with $\mathbf{m_1}$ to get an improved image [equation (16)].

In terms of cost, this approach is comparable to one-and-a-half iterations of a CG method, the first half iteration being the first migration to compute $\mathbf{m_1}$. The cost of estimating the nonstationary filters is negligible compared to the total cost of migration. In the next section, I illustrate this idea with the Marmousi data set. I show that an image similar to the least-squares migration image can be effectively obtained.

MIGRATION RESULTS

I illustrate the proposed algorithm with two data sets where the earth's reflectivity is sought. For $\mathbf{L}'$, I use a prestack split-step double-square root (DSR) migration method with one reference velocity (Stoffa et al., 1990; Popovici, 1996). The forward operator is therefore a DSR modeling operator (Kuhl and Sacchi, 2003). I demonstrate with images migrated at zero offset and with angle-domain common-image gathers (ADCIGs) that the approximation of the Hessian with adaptive filters yields results comparable to least-squares migration.

Poststack migration results

This section illustrates how well the proposed technique recovers the reflectivity of the earth for a simple synthetic data set. Figure 1 shows a reflectivity model as a function of depth.

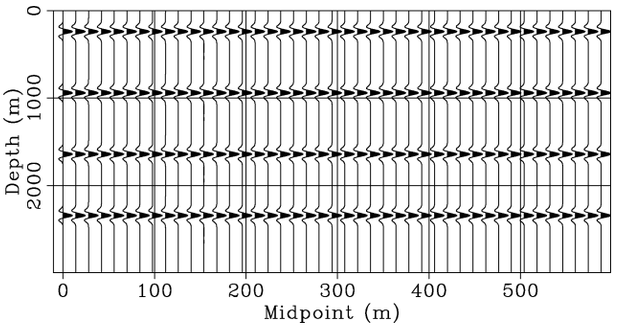

Figure 1. Model reflectivity as a function of depth. The model consists of four flat reflectors with unit amplitude. There is an increment of fourteen between traces.

The reflectivity is kept constant with the midpoint position. It shows four reflectors with unit amplitude. I generate poststack data (Figure 2) from this model with the velocity function of the Marmousi experiment (Figure 3). The density is kept constant. The data are created with the DSR modeling operator. The complex velocity model creates distortion in the wavefield as illustrated in Figure 2. A more realistic way of modeling the data would be with a different operator than the one used for the migration, thus mimicking amplitude issues encountered with field data. In particular, retrieval of the true reflectivity would be more difficult to achieve.

Now we migrate the data in Figure 2 to compute $\mathbf{m_1}$ (Figure 4a), then remodel and remigrate to compute $\mathbf{m_2}$ (Figure 4b). Because the same operator is used to create the data (Figure 2) and to perform the remodeling and migration steps, the migration results are both kinematically correct and have very few artifacts. However, looking closely at the two images in Figure 4, we notice that the amplitudes are affected by the migration. The reflectivity is not constant and equal to one anymore for both $\mathbf{m_1}$ and $\mathbf{m_2}$. This example illustrates that $\mathbf{L}$ is nonunitary.

From the two images $\mathbf{m_1}$ and $\mathbf{m_2}$, a bank of nonstationary filters (Figure 5) is estimated and applied to the migration results $\mathbf{m_1}$. In addition, I run five CG iterations on the same data

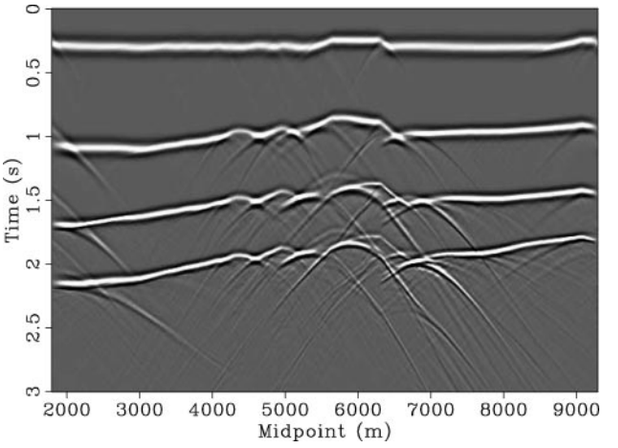

Figure 2. Poststack data created from the reflectivity model in Figure 1 and the velocity field in Figure 3. This data set is generated with the DSR modeling operator.

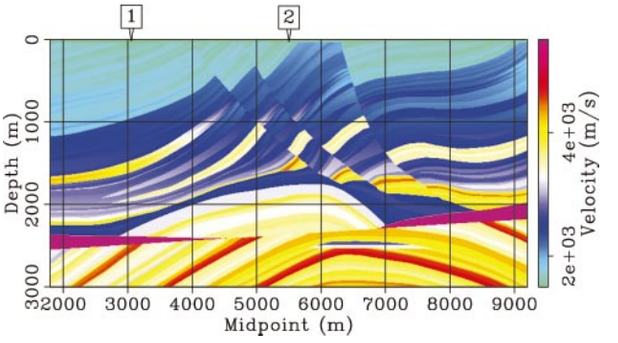

Figure 3. Velocity model for the Marmousi data set. The arrows 1 and 2 correspond to surface locations for the CIGs in Figures 13 and 14.

set. Figure 6 displays a comparison of the imaging results for the filtering technique and the inversion. Both methods yield similar amplitudes by recovering the original reflectivity.

This simple synthetic example illustrates that the migration operator is not unitary and that the proposed approach is able to recover the true reflectivity. Therefore, the nonstationary filters can effectively simulate the inverse of the Hessian. A more realistic comparison would consist in modeling the data in Figure 2 with a different technique than the one used for the inversion, for example, with finite differences. Because only $(\mathbf{L}'\mathbf{L})^{-1}$ is approximated, the modeling of the data itself is not an important issue, however. In the next section, I illustrate the filtering approach with the more difficult Marmousi data set.

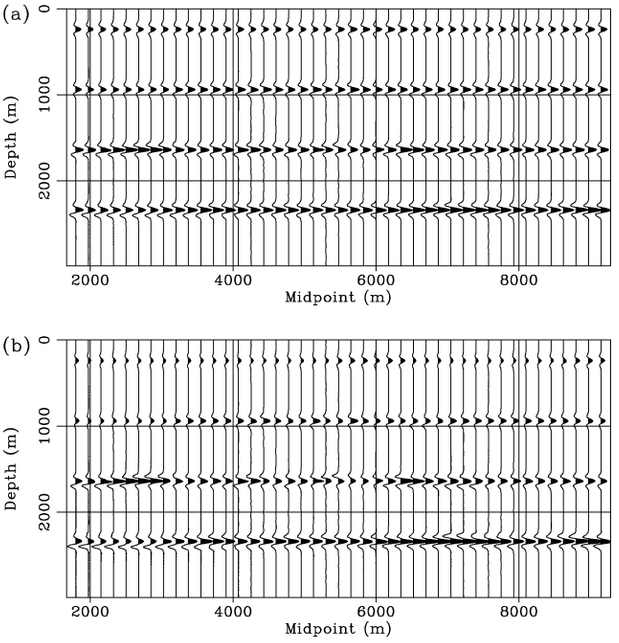

Figure 4. (a) Migration result of the synthetic data set in Figure 2 (i.e., $\mathbf{m_1}$). (b) Migration result of the remodeled data (i.e., $\mathbf{m_2}$). The migration process changes the amplitude of the four flat events.

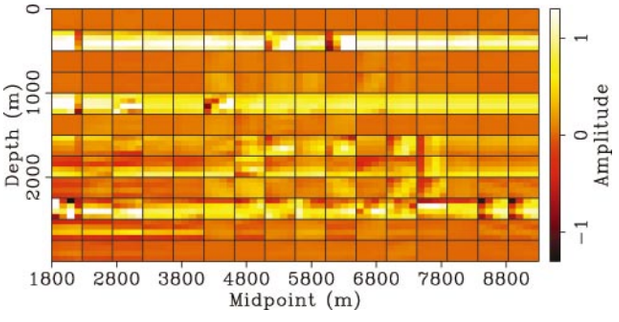

Figure 5. Estimated filters from Figures 4a and 4b. Each cell represents a nonstationary filter with its zero-lag coefficient in the middle. One-fifth of the filters are actually shown in both directions. Each filter position corresponds roughly to a similar area in the migrated image. The size of the filters is 4×4 coefficients. The filter coefficients are the strongest at the four reflector positions.

Zero-offset prestack migration results

Here, we estimate the earth's reflectivity of the Marmousi data set with prestack data. First, I show in Figures 7 and 8 a comparison between the migration result of the Marmousi data set ($\mathbf{m_1}$) and the remodeled data ($\mathbf{m_2}$). We notice that the

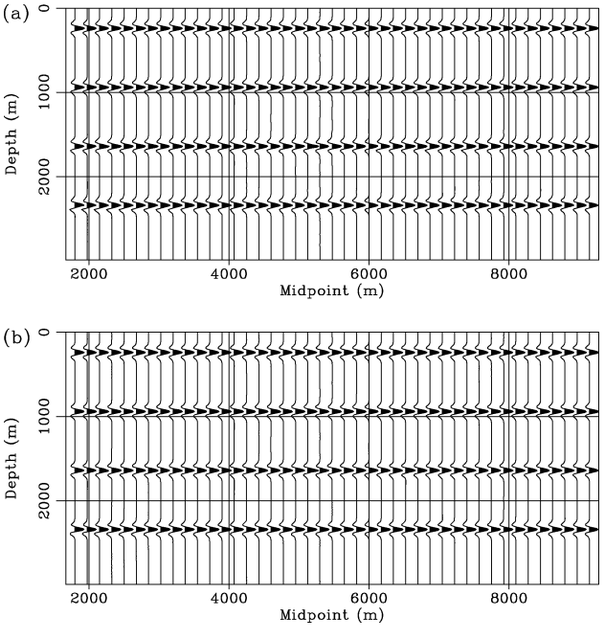

Figure 6. (a) Image estimated after applying the adaptive filters in Figure 5 to $\mathbf{m_1}$ in Figure 4a. (b) Image estimated after five CG iterations. Both methods recover the correct reflection coefficient for each reflector.

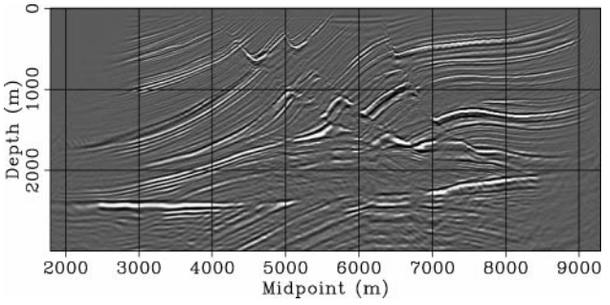

Figure 7. Migration result of the Marmousi data set (i.e., $\mathbf{m_1}$).

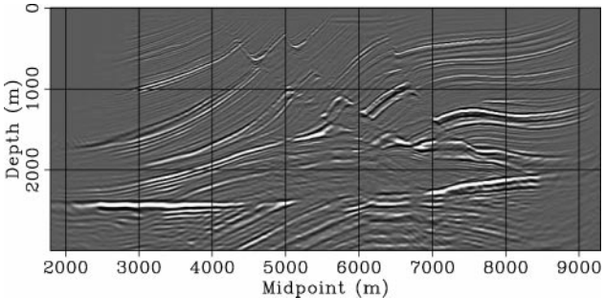

Figure 8. Migration result of the remodeled data from $\mathbf{m_1}$ (i.e., $\mathbf{m_2}$).

migration of the remodeled data (Figure 8) has lower amplitudes in the upper part of the model. Therefore, we expect the filters to correct for this difference. Figure 9 displays a few estimated filters for the Marmousi result. The filters are 10×10 coefficients with 40 patches in depth and 80 patches along the horizontal axis. I show only one-fifth of these filters along both axes. It is interesting to notice that these filters have their highest value at zero lag, meaning that we have a strong amplitude correction with few kinematic changes. The zero-lag values are also larger at the top of the model, as anticipated. Looking more closely at these filters, we see that the coefficients follow the structure of the Marmousi model.

Having estimated filters $\mathbf{b}$ in equation (15), I apply them to $\mathbf{m_1}$ to obtain an improved image. To validate this approach, I show in Figure 10 the result of five CG iterations with the Marmousi data. This results show higher amplitudes at the top, but with inversion artifacts. This problem should be addressed with a proper regularization scheme (Prucha et al., 1999). In Figure 11, I show the corrected image with the approximated Hessian. The amplitude behavior is very similar to Figure 10, without the inversion artifacts.

Note that the filters are not exact impulse responses: they are band-limited filters which depend heavily on the two images $\mathbf{m_1}$ and $\mathbf{m_2}$. As an illustration, two fault-planes shown as F in Figures 10 and 11 are better recovered with least-squares inversion. Finally, I show in Figure 12 the ratio of the smoothed envelopes of Figures 7 and 11. Figure 12 illustrates that the effects of the nonstationary filters (i.e, the Hessian) are stronger on the top of the model. Interestingly, no shadow zones or focusing effects are visible in this image. This proves that the model is well illuminated by the acquisition geometry.

Additionally, the cost of estimating the matching filters is much lower than running five CG iterations. For the Marmousi data set, on eight processors, it took 132 minutes to compute five iterations. For the filtering technique, it took 10 minutes with only one processor to estimate the filters (given $\mathbf{m_1}$ and $\mathbf{m_2}$), which is almost two orders of magnitude faster.

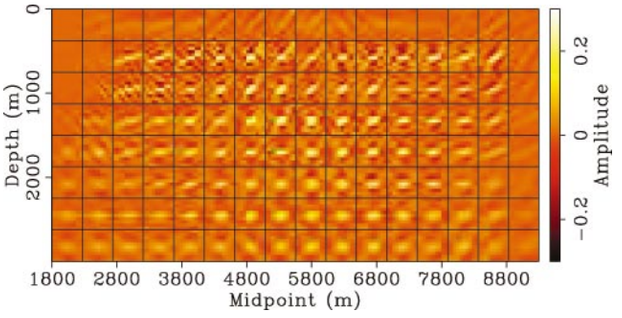

Figure 9. Estimated filters from Figures 7 and 8. Each cell represents a nonstationary filter with its zero-lag coefficient in the middle. One-fifth of the filters are actually shown in both directions. Each filter position corresponds roughly to a similar area in the migrated image. After close inspection of the filter coefficients, these filters seem to follow the structure of the Marmousi model. They are also stronger at the top of the model, as expected.

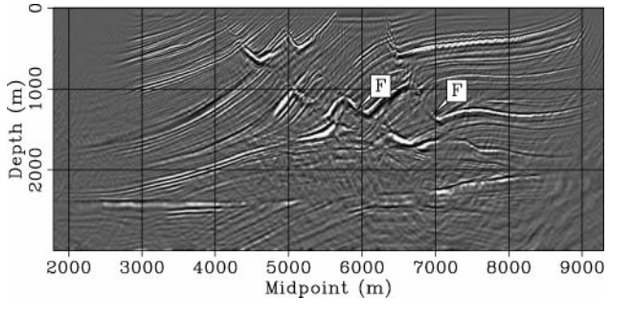

Figure 10. Image estimated after five iterations of CG. The model is noisy because no regularization has been applied during the inversion. Fault planes are indicated by F.

Angle-domain results

As stated in the presentation of the filtering technique, we can apply this method with very different data sets: earth models and imaging operators. In this section, we derive the earth's reflectivity as a function of angle and test our proposed approach in the context of amplitude variation with angle (AVA) estimation. However, it is not the goal of this work to determine if we can recover the true AVA curves. The objective here is to validate the proposed technique with another possible output of the DSR migration method, that is, angle gathers. The angle panels are directly created after migration from the offset panels (Stolt and Weglein, 1985; Weglein and Stolt, 1999; Sava et al., 2001; Sava and Fomel, 2003). The workflow is very similar to the one used in the preceding section:

1) Compute a migrated image $\mathbf{m_1} = \mathbf{L}'\mathbf{d}$ at different offsets, and transform offset gathers into angle gathers.

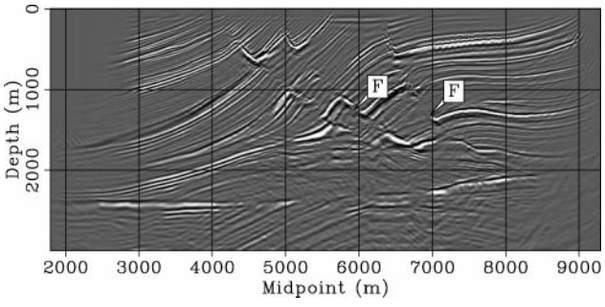

Figure 11. Image estimated after applying the adaptive filters in Figure 9 to $\mathbf{m_1}$ in Figure 7. Amplitudes are similar to the ones observed in Figure 10 without the artifacts. Fault planes are indicated by F.

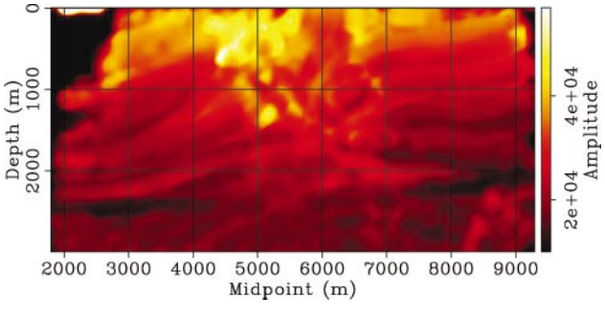

Figure 12. Ratio of the envelopes of Figures 7 and 11. Bright colors correspond to high values. The main effect of the filters is clearly visible at the top.

2) Compute a second image $\mathbf{m_2} = \mathbf{L}'\mathbf{L}\mathbf{m_1}$ at different offsets, and transform offset gathers into angle gathers.
3) Estimate a bank of 2D nonstationary matching filters $\hat{\mathbf{b}}$ for each ADCIG.
4) Convolve $\hat{\mathbf{B}}$ with the corresponding ADCIG from $\mathbf{m_1}$.
5) Stack ADCIGs across angle to form the final image.

I show in Figures 13 and 14 the ADCIGs at two locations of the model (shown as 1 and 2 in Figure 3) for the migration result ($\mathbf{m_1}$), the inversion result after five CG iterations, and the filtering result ($\hat{\mathbf{B}}\mathbf{m_1}$). Again, the angle gather after filtering has fewer artifacts than with inversion, which has a similar amplitude pattern throughout the section. Note that these gathers are not perfectly flat because only one reference velocity is used for this complex model. In Figure 13, the amplitude of the reflectors increases at the top of the section (shown as H in Figures 13b and Figures 13c) and decreases at the bottom (shown as L in Figures 13b and Figures 13c). These observations are consistent with the migrated images at zero offset in Figures 7 and 8. The amplitude of some reflectors increases at large offsets (shown as O). This behavior is similar to what Sava et al. (2001) observed for wave-equation migration with amplitude corrections. In Figure 14, we notice that the filtering approach improves the continuity of some reflectors (shown as C) compared to the inversion result. I display in Figure 15 the estimated filters for the angle gather in Figure 13. Again, we see that we have higher amplitudes for filters at large aperture angles. In addition, we notice a smoothing effects of the filters along the angle axis.

Finally, I show in Figures 16 and 17 stacked images across angle for the CIGs of $\mathbf{m_1}$ and $\mathbf{m_2}$, respectively. The bottom reflectors are stronger than in Figures 7 or 8 with fewer migration

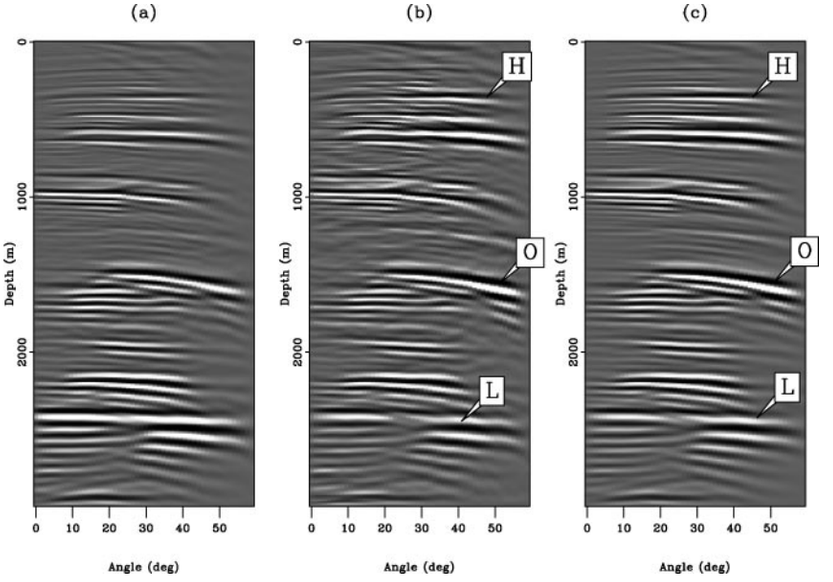

Figure 13. A comparison of migration, inversion, and filtering technique on one common-image gather (CIG). The CIG location is 3050 m (1 in Figure 3). (a) Migration result. (b) Inversion result after five iterations of CG. (c) Filtering result ($\hat{\mathbf{B}}\mathbf{m_1}$). The filtering result is comparable in amplitude to the inversion panel with less artifacts. Hs point to regions of higher amplitudes compared to the simple migration. Ls point to regions of lower amplitudes compared to the simple migration. Os point to regions where the amplitudes increase with angle.

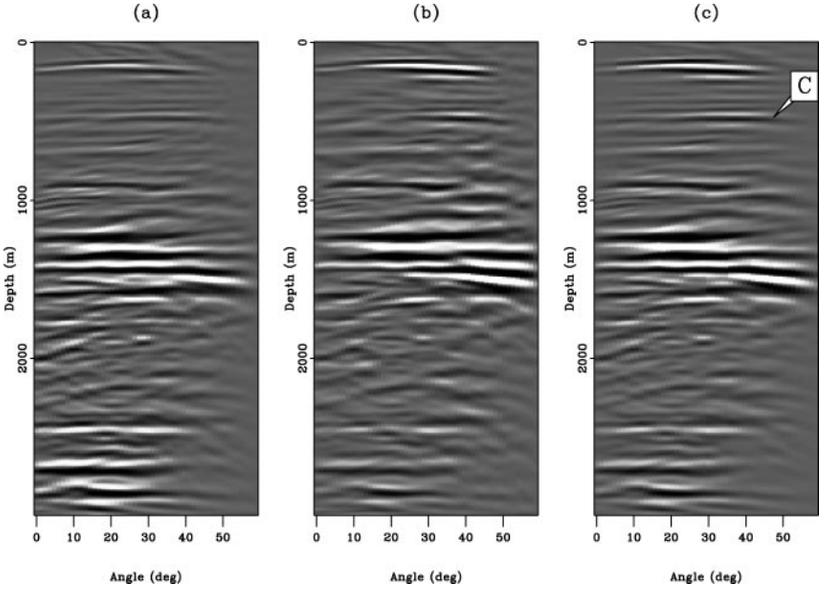

Figure 14. A comparison of migration, inversion, and filtering technique on one CIG. The CIG location is 5550 m (2 in Figure 3). (a) Migration result. (b) Inversion result after five iterations of CG. (c) Filtering result ($\hat{\mathbf{B}}\mathbf{m_1}$). C points to a reflector that is more continuous after filtering than after migration.

artifacts, as expected from the stack. The differences between the two stacked-data panels in Figures 16 and 17 are similar to what we observe between Figures 7 and 8, that is, stronger amplitudes at the top of the image for $\mathbf{m_1}$ and fewer migration artifacts for $\mathbf{m_2}$. Figures 18 and 19 show a comparison between the filtering and inversion approaches for the stacked data. Again, the amplitude pattern is the same for both images, with fewer artifacts in the filtering result (Figure 18).

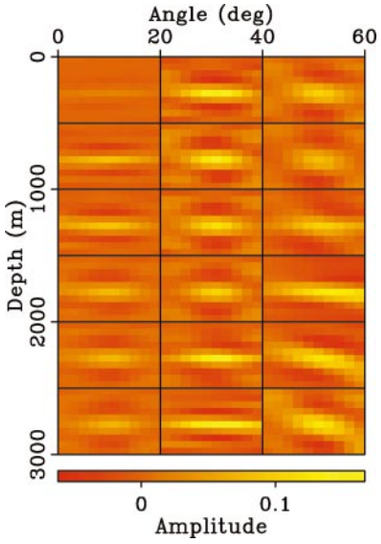

Figure 15. Sample of the estimated matched filters for Figure 13a. One-fifth of the filters are displayed in both directions. Each filter is 10×10. The shapes of these filters prove that they tend to smooth energy along angle.

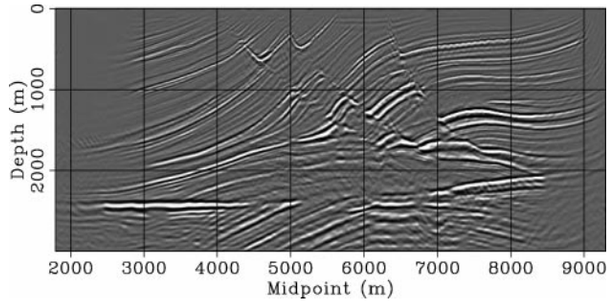

Figure 16. Stacked section of the ADCIGs for the migrated image $\mathbf{m_1}$.

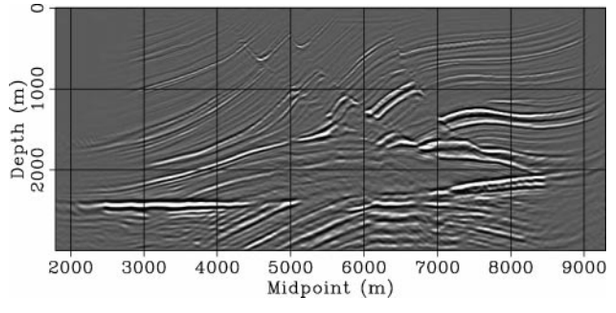

Figure 17. Stacked section of the ADCIGs for the migrated image $\mathbf{m_2}$.

DISCUSSION

In this paper, I presented a method for correcting migrated images by approximating the Hessian of the imaging operator with nonstationary matching filters. These filters are estimated from two migration results. One migrated image, $\mathbf{m_1}$, corresponds to the first migration result. The second image, $\mathbf{m_2}$, is computed by remodeling the data from $\mathbf{m_1}$ and then by remigrating it. It turns out that the relationship between $\mathbf{m_1}$ and $\mathbf{m_2}$ is similar to the relationship that exists between the least-squares inverse $\hat{\mathbf{m}}$ and $\mathbf{m_1}$. In the proposed approach, this relationship is simply captured by matching filters. These filters are not impulse responses. They are spatially band-limited filters constrained by the two images $\mathbf{m_1}$ and $\mathbf{m_2}$ used for the filter estimation step.

I demonstrated with the Marmousi data set that this approach gave a better image than with least-squares without regularization at a lower cost. In addition, this approach is flexible enough to be used on images migrated at zero offset or on ADCIGs. As opposed to Hu et al. (2001), the correction in the image is completely data driven, does not depend on the velocity, and can be applied with any migration operator. It also works in the poststack or prestack domain without any extra effort. Given the data and the computer resources to run at least two migrations to estimate $\mathbf{m_2}$, this method would be easy to apply with 3D migrated images. The helix also makes possible the use of high-dimensionality filters very easily (e.g., 3D) for higher accuracy. Compared to Rickett (2003), this proposed approach does not need reference images. In addition, the multidimensional filters offer more degrees of freedom for the correction than does a simple zero-lag weight in correcting kinematic changes and moving energy locally in the image.

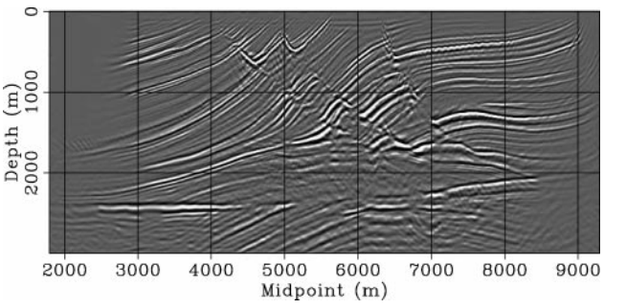

Figure 18. Stacked section of the filtered ADCIGs from $\mathbf{m_1}$.

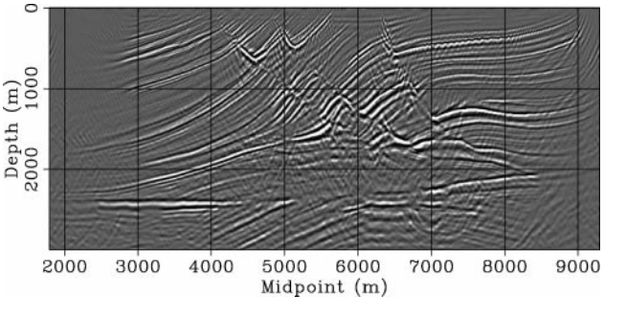

Figure 19. Stacked section of the ADCIGs for the image obtained after five CG iterations.

Kuhl and Sacchi (2003) show that inversion is particularly valuable to attenuate artifacts from acquisition footprint by applying a regularization in the ADCIGs. The proposed filtering technique can be easily adapted to this case by adding a second term in equation (7) as follows:

$$\mathbf{m_2} = (\mathbf{L}'\mathbf{L} + \epsilon^2\mathbf{A}'\mathbf{A})\mathbf{m_1}, \tag{17}$$

where $\mathbf{A}$ is a regularization operator and ϵ a trade-off parameter. The roughening operator can be a simple gradient in the angle domain or filters with geological constraints (Clapp and Biondi, 2002). These possibilities are subject of future research. Alternatively, these filters can be used as preconditioning operators providing faster convergence for iterative inversion.

ACKNOWLEDGMENTS

I thank Paul Sava for providing the migration codes, and the sponsors of the Stanford Exploration Project for their financial support. I also thank Tamas Nemeth, Yonghe Sun, and the reviewers for their constructive comments.

REFERENCES

Beylkin, G., 1985, Imaging of discontinuities in the inverse scattering problem by inversion of a causal generalized Radon transform: Journal of Mathematical Physics, **26**, 99–108.

Bleistein, N., 1987, On the imaging of reflectors in the earth: Geophysics, **52**, 931–942.

Bourgeois, A., Bourget, M., Lailly, P., Poulet, M., Ricarte, P., and Versteeg, R., 1991, Marmousi, model and data: Proceedings of 1990 EAEG Workshop on Practical Aspects of Seismic Data Inversion.

Claerbout, J. F., 1985, Imaging the earth's interior: Blackwell Scientific Publications.

——— 1992, Earth soundings analysis, processing versus inversion: Blackwell Scientific Publications.

——— 1998, Multidimensional recursive filters via a helix: Geophysics, **63**, 1532–1541.

Clapp, M., and Biondi, B., 2002, Subsalt event regularization with steering filters: 72nd Annual International Meeting, SEG, Expanded Abstracts, 1176–1179.

Fomel, S., Sava, P., Rickett, J., and Claerbout, J., 2003, The Wilson-Burg method of spectral factorization with application to helical filtering: Geophysical Prospecting, **51**, 409–420.

Gray, S. H., 1997, True-amplitude seismic migration: A comparison of three approaches: Geophysics, **62**, 929–936.

Guitton, A., and Verschuur, D., 2004, Adaptive subtraction of multiples using the L_1-norm: Geophysical Prospecting, **52**, 27–38.

Hu, J., Schuster, G. T., and Valasek, P., 2001, Poststack migration deconvolution: Geophysics, **66**, 939–952.

Kostov, C., 1990, Toeplitz structure in slant-stack inversion: 60th Annual International Meeting, SEG, Expanded Abstracts, 1618–1621.

Kuhl, H., and Sacchi, M., 2001, Generalized least-squares DSR migration using a common angle imaging condtion: 71st Annual International Meeting, SEG, Expanded Abstracts, 1025–1028.

——— 2003, Least-squares wave-equation migration for AVP/AVA inversion: Geophysics, **68**, 262–273.

Lambaré, G., Virieux, J., Madariaga, R., and Jin, S., 1992, Iterative asymptotic inversion in the acoustic approximation: Geophysics, **57**, 1138–1154.

Margrave, G. F., 1998, Theory of nonstationary linear filtering in the Fourier domain with application to time-variant filtering: Geophysics, **63**, 244–259.

Mersereau, R. M., and Dudgeon, D. E., 1974, The representation of two-dimensional sequences as one-dimensional sequences: IEEE Transaction on Acoustic, Speech, and Signal Processing, **22**, 320–325.

Nemeth, T., Wu, C., and Schuster, G. T., 1999, Least-squares migration of incomplete reflection data: Geophysics, **64**, 208–221.

Popovici, A. M., 1996, Prestack migration by split-step DSR: Geophysics, **61**, 1412–1416.

Prucha, M., Biondi, B., and Symes, W., 1999, Angle-domain common image gathers by wave-equation migration: 69th Annual International Meeting, SEG, Expanded Abstracts, 824–827.

Rickett, J., 2003, Illumination-based normalization for wave-equation depth migration: Geophysics, **68**, 1371–1379.

Rickett, J., Guitton, A., and Gratwick, D., 2001, Adaptive multiple subtraction with non-stationary helical shaping filters: 63rd Annual Meeting, European Association of Geoscientists and Engineers, Expanded Abstracts, P167.

Sava, P., Biondi, B., and Fomel, S., 2001, Amplitude-preserved common image gathers by wave-equation migration: 71st Annual International Meeting, SEG, Expanded Abstracts, 296–299.

Sava, P., and Fomel, S., 2003, Angle-domain common-image gathers by wavefield continuation methods: Geophysics, **68**, 1065–1074.

Stoffa, P. L., Fokkema, J. T., de Luna Freire, R. M., and Kessinger, W. P., 1990, Split-step Fourier migration: Geophysics, **55**, 410–421.

Stolt, R. H., and Weglein, A. B., 1985, Migration and inversion of seismic data: Geophysics, **50**, 2458–2472.

Thierry, P., Operto, S., and Lambaré, G., 1999, Fast 2-D ray + Born migration/inversion in complex media: Geophysics, **64**, 162–181.

Weglein, A. B., and Stolt, R. H., 1999, Migration-inversion revisited: The Leading Edge, **18**, 950–952.